Published by :
http://www.ijert.org

International Journal of Engineering Research & Technology (IJERT)
ISSN: 2278-0181
Vol. 14 Issue 03, March-2025

Effect of PA66 Dip Coating Process on Wind Turbine Pitch Bearing Cage

Zhiwei Sun, Yanshuang Wang
School of Mechanical Engineering, Qilu University of Technology (Shandong Academy of Sciences)
Jinan 250353, China

Guanghui Zheng, Ximing Yuan,
Shandong Golden Empire Precision Machinery Technology Co., Ltd.

***Abstract*—With the development and application of wind turbine pitch bearings, the performance and service life of bearings have become particularly important. The bearing cage, as a critical component in the bearing, has a significant impact. The material used in this study was nylon 66 (PA66). Samples under different dip coating process parameters were subjected to porosity, thickness, and density tests, friction and wear tests, and related characterizations. The influence mechanisms of preheating temperature, dip coating time and vulcanizing temperature on the porosity, thickness, and density of the cages were analyzed. Additionally, the impact mechanisms of porosity, thickness, and density on the friction and wear performance of the cage were examined. The optimal process parameters were determined by establishing an optimization model. The results show that by appropriately controlling the preheating temperature, dip coating time, and vulcanizing temperature, it is possible to produce a smooth and uniform dip coating layer with good compactness, thereby effectively improving the friction and wear properties of the dip coating bearing cage.The optimal combination of process parameters for dip coating bearing cage is: preheating temperature of 430.72 ℃, dip coating time of 8.05 s, and vulcanizing temperature of 199.18 ℃.**

***Keywords*—dip coating process; nylon 66; friction and wear performance; optimize model**

I. INTRODUCTION

Wind power generation is a kind of clean renewable energy. Developing wind power generation is of great significance for solving energy crisis, reducing environmental pollution and regulating energy structure. Bearings are the key component of the wind turbine [1]. The cage is the more critical component of the rolling bearing, which has a significant impact on the performance and life of the bearing. In practical applications, under the high-speed rotation and changing working environment of wind turbines, the cage is subjected to frequent impacts, which leads to the formation and expansion of fatigue cracks. At the same time, the bearing cage affected by external factors such as corrosion and high temperature, which can accelerate the aging and failure of the cage. In order to avoid bearing failure and extend its life, selecting the appropriate surface technology treatment method is the key to reduce bearing failure [2].

The dip coating process has a series of advantages in the surface treatment of hard materials such as easy forming, uniform covering and increased wear resistance [3]. By coating the surface of the bearing cage with a wear-resistant plastic product, the contact between the bearing cage and the rolling elements becomes plastic-to-steel rather than steel-to-steel, which improves the friction environment and reduces the friction coefficient [4]. The impact resistance, corrosion resistance, wear resistance and service life of the bearing cage after dip coating have been significantly improved [5, 6], and the noise is reduced, which can meet the use of cold and humid climates, especially improving the impact performance of low temperature environment. It has been widely studied and applied in different fields in recent years [7, 8, 9].

Currently, the impact of dip coating process on the performance of bearing cages has not been studied by scholars. In this paper, PA66 was selected as the dip coating material, and bearing cage samples with different process parameters were prepared. Porosity, thickness and density tests, friction and wear tests, and related characterizations were conducted. The influence mechanisms of three dip coating process parameters, preheating temperature, dip coating time and vulcanizing temperature on the porosity, thickness, and density of the cages were analyzed based on the experimental data and characterization results. Additionally, the impact mechanisms of porosity, thickness, and density on the friction and wear performance of the cage were examined. The optimal process parameters were determined by establishing an optimization model. This study applies the dip coating process to wind power bearing cages, enhancing their wear resistance and friction-reducing capabilities, expanding the application range of the dip coating process, and significantly improving the overall performance of the bearings, making them more suitable for various working conditions and application requirements.

II. MATERIALS AND METHODS

A. Dip coating materials

The dip coating material studied in this paper is PA66, which is a thermoplastic resin. Hexanedioic acid and hexamethylene diamine react to form PA66 salt, which then undergoes polycondensation to produce PA66. The reaction process is illustrated in Fig. 1.

Published by :
http://www.ijert.org

International Journal of Engineering Research & Technology (IJERT)
ISSN: 2278-0181
Vol. 14 Issue 03, March-2025

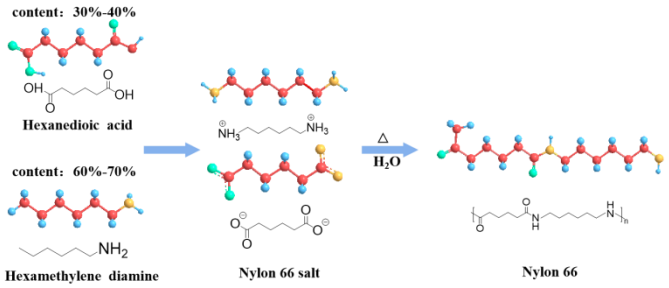

Fig. 1. Reaction process diagram of hexanedioic acid and hexamethylene diamine producing PA66.

PA66 is a partially crystalline polymer material. Its molecular chain contains relatively long units of hexanedioic acid and hexamethylene diamine, which can form an ordered structure during crystallization. This ordered structure gives PA66 a high degree of crystallinity and a relatively ordered molecular arrangement. Additionally, the long-chain units of hexanedioic acid and hexamethylene diamine in the PA66 molecular chain interact through weak forces such as hydrogen bonds and van der Waals forces, forming a relatively stable intermolecular structure [10].

B. Preparation of dip coating samples

Firstly, the undip coating cage samples are placed into a sandblasting machine for cleaning to remove oil stains and rust from the surface. Subsequently, the cage samples undergo a preheating treatment. Then, the preheated cage samples are immersed into molten PA66 to form a coating of a certain thickness. After that, the dip coating cage samples are placed into an oven for curing. Finally, the dip coating cage samples are put into a vulcanizing bed for vulcanization [11]. Once cooled and dried, the dip coating cage samples are obtained. The preparation process of the dip coating cage sample is shown in Fig. 2.

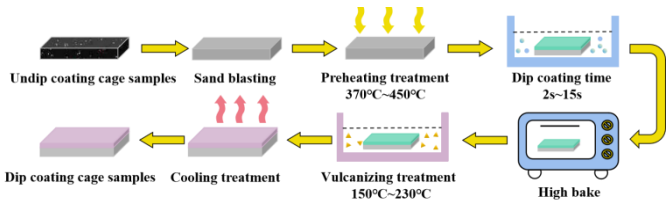

Fig. 2. Process flow diagram for the preparation of dip coating cage samples.

C. Process parameter design

This study utilizes the orthogonal experiment method to arrange the combinations of key factors and levels. Orthogonal experimental design is generally organized using an orthogonal table, which is a complete set of standardized design forms typically represented as Ln(tc). Here, n represents the number of factors in the experiment, and t denotes the number of levels for the orthogonal experiment.

A 3-factor, 5-level orthogonal table L25(35) is used to design the process parameters. The corresponding parameter levels are shown in Table 1.

Table 1 Orthogonal experimental factor level table.

Level	Preheating temperature (℃)	Dip coating time (s)	Vulcanizing temperature (℃)
1	370	2	150
2	390	5	170
3	410	9	190
4	430	12	210
5	450	15	230

D. Porosity, thickness, and density tests

Porosity refers to the ratio of voids present within a material. The porosity test employs a microscopic measurement method. As shown in Fig. 3(a-b), a metallographic microscope (MIT300) is utilized to observe and capture images of the void structures on the surface of the dip coating layer. Image processing software is then used to analyze the area and distribution of the pores. The porosity of the dip coating layer is determined using formula (1).

$$\varphi = \frac{A_p}{A_t} \times 100\% \quad (1)$$

A_p is the total area of pores, and A_t is the total area of the sample, φ is the porosity.

The thickness measurement was conducted using a microscopic measurement method. A metallographic microscope (MIT300) was used to observe the cross-section of the cut sample. The results are shown in Fig. 3(c-d). The measurement scale of the microscope was utilized to accurately measure the thickness of the dip coating layer.

The density test was conducted using the Archimedes' principle, which involves measuring the change in buoyant force of the plasticized layer in water to calculate the density of the object. The calculation method is formula (2).

$$\rho = \frac{W}{W - W_l} \times \rho_l \quad (2)$$

W is the weight of the sample, W_l is the weight of the sample in water, ρ is the density of the sample, and ρ_l is the density of water.

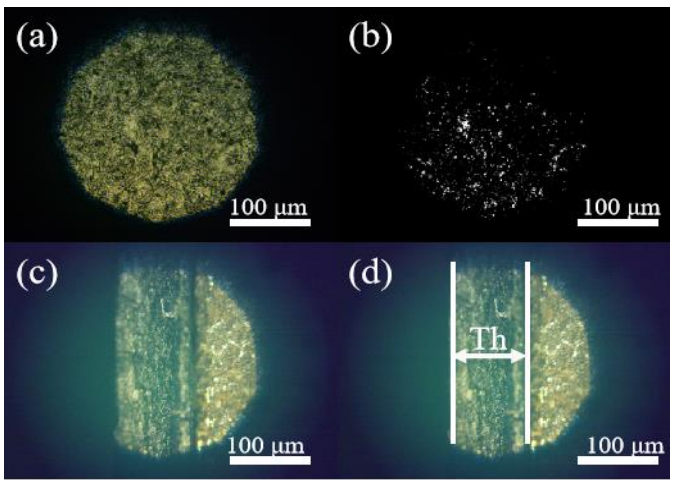

Fig.3 (a-b) Measurement of porosity. Fig.3 (c-d) Measurement of thickness.

International Journal of Engineering Research & Technology (IJERT)
ISSN: 2278-0181
Vol. 14 Issue 03, March-2025

E. Friction and wear tests

The friction and wear properties of the dip coating samples were tested using a UMT-TriboLab friction and wear testing machine. Fig. 4(a) shows the upper and lower samples used in the experiment, with the specific parameters of the upper and lower samples listed in Table 2. The yellow part in the magnified section of Fig. 4(b) represents the glass fiber reinforced material, which primarily serves to connect and form long-chain polymers, creating a stable, high-strength structure. The black parts represent carbon black, used to enhance its mechanical properties. Before testing, the testing ball and dip coating sample were ultrasonically cleaned in anhydrous ethanol for 15 minutes. The friction testing period was set to 20 minutes, and after the test, both the ball and the dip coating cage sample were ultrasonically cleaned for 10 minutes to analyze the wear surface. Three tests were conducted for each sample to reduce testing errors. Detailed information on the tribological tests can be found in Table 3.

Table 2 Upper and lower test simple parameters.

Material	Dimension	Surface roughness(Ra)	Hardness
GCr15	Diameter 6 mm	0.22 μm	750 HV
Dip PA66 coating	30×50×5mm	0.7 μm	100 HV

Table 3 Tribological experimental details of UMT-TriboLab.

Test conditions	
Contact load (N)	20, 100
Maximum hertzian contact pressure (GPa)	0.11, 0.18
Frequency (Hz)	3
Ambient temperature (℃)	20
Distance (cm)	1

F. Characterization and analysis

The surface morphology of the dip coating cage sample was observed using a super-depth three-dimensional observation microscopic system (VHX-5000). At the same time, a scanning electron microscope (FE-SEM, Sigma 300) was utilized to examine the microstructural changes of the dip coating cage sample. An energy-dispersive X-ray spectrometer (EDS, Phenom Prox) was used to analyze the elemental content and chemical state of the wear surface.

III. RESULT AND DISCUSSION

A. The influence mechanism of porosity

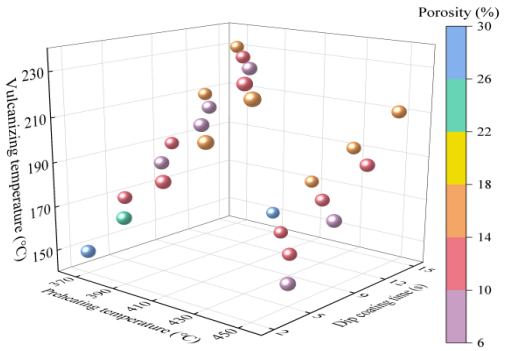

Fig. 5 Porosity under different dip coating process parameter combinations.

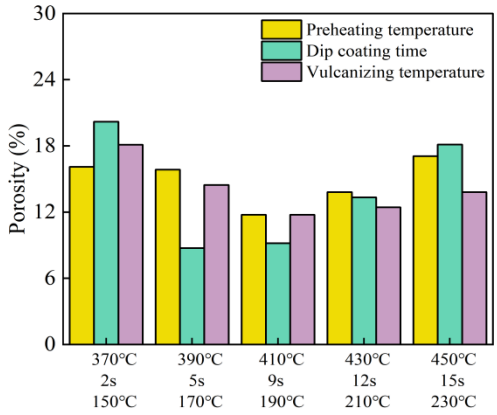

Fig.6 Effect of dip coating process parameters on porosity.

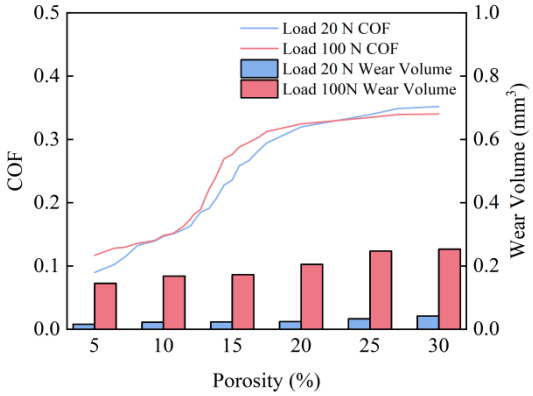

Fig.7 Effect of dip coating layer porosity on friction coefficient and wear volume.

From Fig. 5-6, it can be observed that the porosity of the dip coating layer initially decreases and then increases with the rise in preheating temperature, dip coating time, and vulcanizing temperature. When they are relatively low, PA66 cannot fully melt, resulting in insufficient coating of the dip coating layer on the substrate surface and hindering curing. The vulcanizing rate decreases, and the surface fluidity of the dip coating layer becomes poor, making it difficult to form. These factors collectively lead to an increase in porosity. As the preheating temperature, dip coating time, and vulcanizing temperature increase, PA66 gradually melts uniformly, allowing generated bubbles to be effectively expelled and promoting curing. With a moderate vulcanizing rate and uniform vulcanizing reactions. The above reasons lead to a reduction in porosity. However, when they are excessively high, PA66 over melts, causing bubbles to become trapped, and the surface of the dip coating layer cures prematurely. The vulcanizing rate becomes too fast, resulting in uneven reaction rates and localized over vulcanization. These factors contribute to an increase in porosity.

From Fig. 7, it can be seen that the friction coefficient and wear volume of the dip coating cage increase with the rise in the porosity of the dip coating layer. When the porosity is low, the surface of the dip coating layer is denser, enabling it to better withstand the pressure and heat generated by friction. This helps improve the compressive strength and wear resistance of the dip coating sample, reducing the friction coefficient and wear volume. An increase in porosity indicates the presence of more voids or microcracks within the material. The air or gas trapped in these pores hinders heat transfer. As a result, the heat generated during the friction process is more likely to

Published by :
http://www.ijert.org

International Journal of Engineering Research & Technology (IJERT)
ISSN: 2278-0181
Vol. 14 Issue 03, March-2025

accumulate on the surface, leading to excessive temperatures. This exacerbates wear or softening of the dip coating layer, causing a decline in local surface strength, thereby increasing the friction coefficient and wear volume.

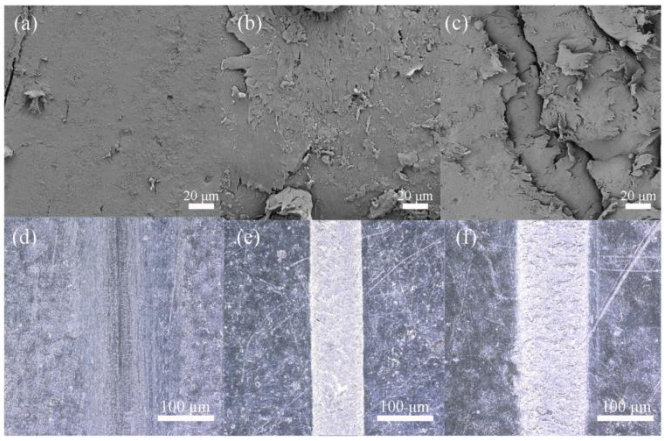

Fig. 8(a-c) SEM images of wear surfaces at 10%, 20%, and 30% porosities. Fig. 8(d-f) surface morphology dip coating samples at 10%, 20%, and 30% porosities.

To clarify the wear mechanisms of dip coating cage samples under different porosity levels, samples with varying porosity were selected for further analysis. Fig. 8(a-c) and (d-f) show the SEM images and the wear surface morphology of dip coating cage samples after wear. 6(a) and (d), it can be observed that the wear surfaces of dip coating cage samples prepared with lower porosity are smoother, with only some grooves and minimal tearing observed on the surface, indicating that the primary wear mechanism is abrasive wear. From Fig. 8(b-c) and (e-f), it is evident that as the porosity increases, the wear surfaces of the prepared dip coating cage samples exhibit more tearing, suggesting intensified surface wear. Additionally, numerous grooves can be seen on the wear surfaces, as the presence of pores and microcracks facilitates localized material spalling, leading to aggravated wear. Therefore, the wear mechanisms are identified as adhesive wear and abrasive wear.

B. The influence mechanism of thickness

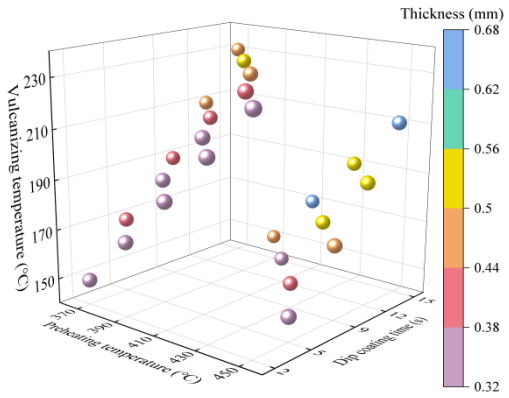

Fig. 9 Thickness under different dip coating process parameter

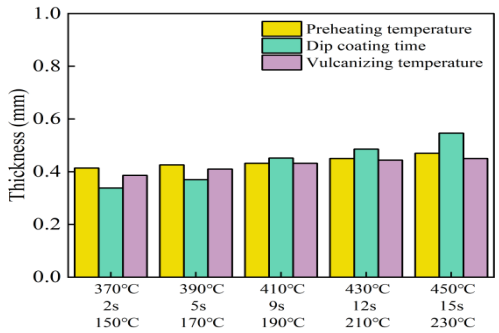

Fig. 10 Effect of dip coating process parameters on thickness.

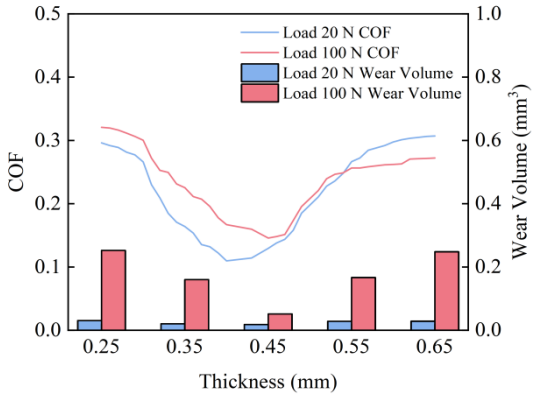

Fig. 11 Effect of dip coating layer thickness on friction coefficient and wear volume.

From Fig. 9-10, it can be observed that the thickness of the dip coating layer increases with the rise in preheating temperature, dip coating time, and vulcanizing temperature. When they are relatively low, PA66 absorbs less heat, making it difficult to effectively adhere to the substrate. The loose structure of the dip coating layer results in an incomplete curing. These factors contribute to a thinner dip coating layer. As the preheating temperature, dip coating time, and vulcanizing temperature increase, the surface temperature of the dip coating layer rises, allowing PA66 to melt more easily and adhere to the substrate surface, ensuring thorough curing of the dip coating layer. These factors ensure a smooth and uniform thickness of the dip coating layer. However, when they are excessively high, an excessive amount of PA66 adheres to the substrate surface, leading to localized accumulation. The surface of the dip coating layer cures too quickly, while the interior may not be fully melted. These factors result in an overly thick and uneven dip coating layer.

From Fig. 11, it can be observed that the friction coefficient and wear volume of the dip coating cage initially decrease and then increase with the rise in the thickness of the dip coating layer. When the thickness is relatively low, the dip coating layer cannot fully fill the microscopic irregularities on the substrate surface. This results in a larger contact area and higher friction between the upper sample and the dip coating layer, leading to increased heat generation and a rise in the friction coefficient and wear volume. As the thickness increases, the dip coating layer better fills the surface irregularities of the substrate, increasing the contact area between the upper sample and the dip coating layer, thereby providing improved friction performance and resulting in a

Published by :
http://www.ijert.org

International Journal of Engineering Research & Technology (IJERT)
ISSN: 2278-0181
Vol. 14 Issue 03, March-2025

reduction in the friction coefficient and wear volume. However, when the thickness becomes excessively high, the dip coating layer absorbs too much heat. This reduces the bonding strength between the substrate and the dip coating layer, leading to an increase in the friction coefficient and wear volume.

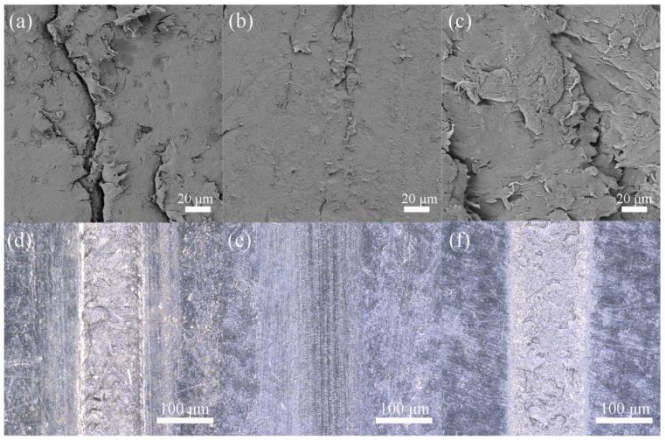

Fig. 12(a-c) SEM images of wear surfaces at 0.35 mm, 0.45 mm, and 0.55 mm thicknesses.
Fig. 12(d-f) surface morphology dip coating samples at 0.35 mm, 0.45 mm, and 0.55 mm thicknesses.

To clarify the wear mechanisms of dip coating cage samples under different thicknesses, samples with varying thicknesses were selected for further analysis. Fig. 12(a-c) and (d-f) show the SEM images and wear surface morphology of dip coating cage samples. From Fig. 12(a), (c-d), and (f), it can be observed that the wear surfaces of dip coating cage samples prepared with excessively thin or thick dip coating layers exhibit more tearing. A thinner dip coating layer often fails to effectively dissipate heat and pressure, leading to localized thermal fatigue, cracks, and spalling. The wear patterns manifest as significant micro-wear and peeling. When the thickness is excessively large, numerous grooves can be seen on the wear surfaces, indicating intensified surface wear of the dip coating cage samples. From Fig. 12(b) and (e), Only some grooves and minimal tearing are observed on the surface of the dip coating cage samples. In this case, the contact mode of the friction surface may resemble adhesive contact, and the wear pattern changes, primarily exhibiting surface spalling or scratching, with a potential reduction in wear volume.

C. The influence mechanism of density

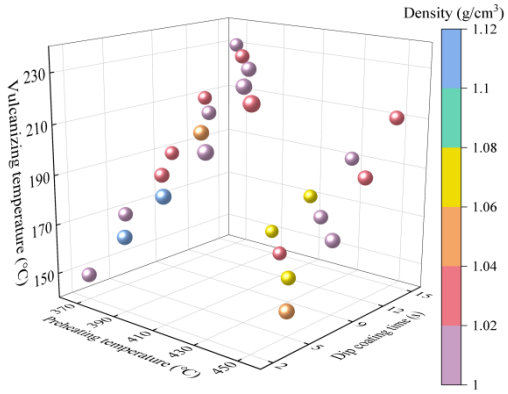

Fig. 13 Density under different dip coating process parameter combinations.

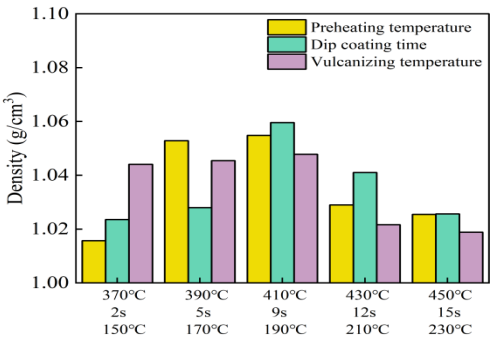

Fig. 14 (b) Effect of dip coating process parameters on density.

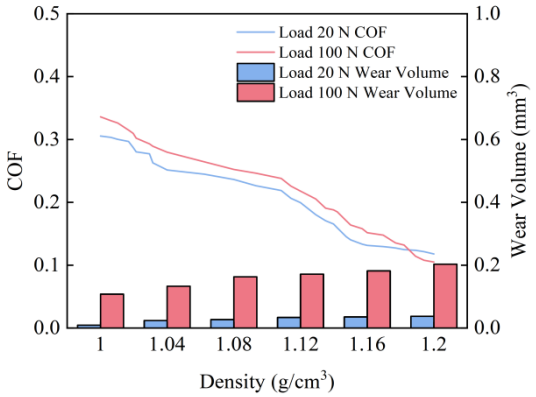

Fig. 15 Effect of dip coating layer density on friction coefficient and wear volume.

From Fig. 13-14, it can be observed that the density of the dip coating layer initially increases and then decreases with the rise in preheating temperature, dip coating time, and vulcanizing temperature. When they are relatively low, the presence of bubbles and unmelted PA66 within the dip coating layer results in a loose internal structure, leading to a reduction in density. As the preheating temperature, dip coating time, and vulcanizing temperature increase, PA66 melts uniformly, creating a smooth surface and a dense internal structure in the dip coating layer, thereby increasing its density. However, when they are excessively high, an excessive accumulation of PA66 may lead to incomplete melting within the dip coating layer, trapping internal bubbles and potentially increasing porosity, which causes a decline in density.
From Fig. 15, it can be seen that the friction coefficient and wear volume of the dip coating cage decrease as the density increases. When the density is low, the internal structure of the dip coating layer is loose, with high porosity and a rough, soft surface, resulting in a higher friction coefficient and wear volume. As the density increases, the internal structure of the dip coating layer becomes denser, reducing localized plastic deformation and creating a smoother surface. This decreases the contact area with the upper sample, leading to a reduction in the friction coefficient and wear volume.

International Journal of Engineering Research & Technology (IJERT)
ISSN: 2278-0181
Vol. 14 Issue 03, March-2025

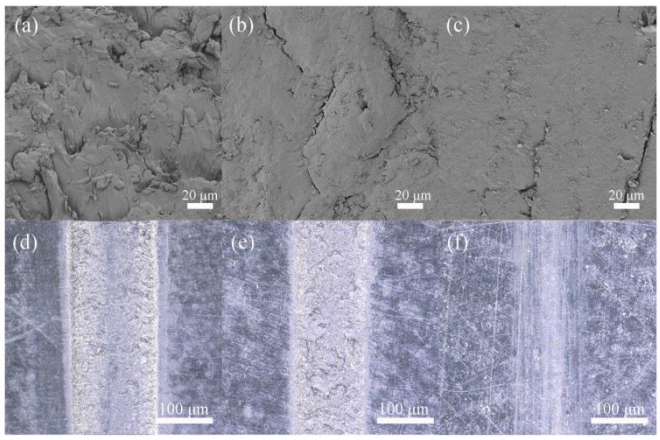

Fig. 16(a-c) SEM images of wear surfaces at 1.02 g/cm^3, 1.08 g/cm^3, and 1.14 g/cm^3 densities.
Fig. 16(d-f) surface morphology dip coating samples 1.02 g/cm^3, 1.08 g/cm^3, and 1.14 g/cm^3 densities.

To clarify the friction and wear mechanisms of dip coating cage samples under different densities, samples with varying densities were selected for further analysis. Fig. 16(a-c) and (d-f) show the SEM images and the surface wear morphology of each dip coating cage sample after wear under different densities. From Fig. 16(a-b) and (d-e), it can be observed that the wear surfaces of dip coating cage samples prepared with lower densities exhibit intensified wear, with numerous grooves visible on the wear surfaces. Therefore, the wear mechanisms include adhesive wear, fatigue wear, and abrasive wear. From Fig. 16(c) and (f), it can be seen that as the density increases, the wear surfaces of the prepared dip coating cage samples become smoother. Only some grooves and minimal tearing are observed on the surfaces, indicating that the primary wear mechanism is abrasive wear.

IV. DETERMINATION OF THE BEST PROCESS PARAMETERS OF DIPPING

To determine the relationship between dip coating process parameters and the porosity, thickness, and density, a mathematical model for the porosity, thickness, and density as functions of the dip coating process parameters was established, as shown in formula (3).

$$y = \beta_0 + \sum_{j=1}^{k} \beta_j x_j + \sum_{j=1}^{k} \beta_{jj} x_j^2 + \sum_{i=1}^{k-1} \sum_{j=i+1}^{k} \beta_{ij} x_i x_j \quad (3)$$

The predicted results are shown in formulas (4), (5), and (6). φ is porosity, *Th* is thickness, ρ is density, p is preheating temperature, t is dip coating time, and v is vulcanizing temperature.

$$\varphi = 94 + 1.12p + 7.6t - 3.52v - 0.0029p^2 + 0.088t^2 - 0.00128v^2 - 0.0404pt + 0.00857pv + 0.0421tv \quad (4)$$

$$Th = -1.27 + 0.0116p + 0.054t - 0.0125v - 0.000024p^2 - 0.00095t^2 - 0.00038v^2 - 0.000207pt + 0.000058pv + 0.000352tv \quad (5)$$

$$\rho = -3.13 + 0.0186p + 0.006t + 0.0039v - 0.000021p^2 + 0.00066t^2 - 0.00001v^2 - 0.000069pt - 0.000002pv + 0.00005tv \quad (6)$$

To objectively reflect the degree of influence of porosity, thickness, and density on the dip coating process, weight coefficients were used for evaluation. The method chosen for calculating the weight coefficients is the Analytic Hierarchy Process (AHP) [12]. The results are shown in Table 4.

Table 4 results of the weight coefficient

	Porosity	Thickness	Density
Weight coefficient	90.42%	2.85%	6.73%

Using the obtained mathematical models of porosity, thickness, and density as functions of the dip coating process parameters as the objective functions, a weighted summation approach was employed to transform the multi-objective problem into a single-objective problem. The single-objective function is given by formula (7).

$$F(p,t,v) = -84 - 1.003218p - 6.83796t + 3.167898v + 0.002608p^2 - 0.079182t^2 + 0.00115v^2 + 0.036349pt - 0.007711pv - 0.037876tv \quad (7)$$

Find the extremum points of formula (7). The obtained extremum points represent the optimal dip coating process parameters. The results are as follows: preheating temperature is 430.72 ℃, dip coating time is 8.05 s, and vulcanizing temperature is 199.18 ℃.

V. CONCLUSION

During the dip coating process, the process parameters significantly influence the porosity, thickness, and density. By appropriately controlling the preheating temperature, dip coating time, and vulcanizing temperature, it is possible to produce a smooth and uniform dip coating layer with good compactness, thereby effectively improving the friction and wear properties of the dip coating bearing cage.
The optimal process parameters for the dip coating bearing cage are as follows: preheating temperature of 430.72 ℃, dip coating time of 8.05 s, and vulcanizing temperature of 199.18 ℃.

ACKNOWLEDGMENT

The work is supported by the projects funded by the National Natural Science Foundation of China (52075274 and 51475143), the Shandong Provincial Key Research and Development Program (Major Science and Technology Innovation Project) (2020CXGC011003) and Taishan Industrial Experts Programme (tscx202312171).

REFERENCES

[1] A. Dhanola, and H. C. Garg, “Tribological challenges and advancements in wind turbine bearings: A review,” Engineering Failure Analysis, 118, 104885, September 2020. https://doi.org/10.1016/j.engfailanal.2020.104885.
[2] H. Chen, H. Zhang, H. Liang, and W. Wang, “The collision and cage stability of cylindrical roller bearing considering cage flexibility,” Tribology International, 192, 109219, April 2024. https://doi.org/10.1016/j.triboint.2023.109219.
[3] X. Tang, and X. Yan, “Dip-coating for fibrous materials: mechanism, methods and applications,” Journal of Sol Gel Science & Technology, 81(2), 378-404, September 2016. https://doi.org/10.1007/s10971-016-4197-7.
[4] L. Zsidai, P. Samyn, K. Vercammen, K. Van Acker, M. Kozma, G. Kalácska, and P. De Baets, “Friction and Thermal Effects of Engineering Plastics Sliding Against Steel and DLN-Coated Counterfaces,” Tribology Letters, 17(2), 296-288, August 2004. https://doi.org/10.1023/B:TRIL.0000032453.09366.d4.

International Journal of Engineering Research & Technology (IJERT)
ISSN: 2278-0181
Vol. 14 Issue 03, March-2025

[5] R. J. M. Borggreve, R. J. Gaymans, and J. Schuijer, “Impact behaviour of nylon-rubber blends: 5. Influence of the mechanical properties of the elastomer,” Polymer, 30(1), 71-77, January 1989. https://doi.org/10.1016/0032-3861(89)90385-6.

[6] H. Chen, H. Zhao, J. Qu, H. Shao, and S. Zhao, “Erosion–corrosion of thermal-sprayed nylon coatings,” Wear, 233, 431-435, December 1999. https://doi.org/10.1016/S0043-1648(99)00234-3.

[7] S. Mahadik, V. Parale, R. Vhatkara, D. Mahadik, M. Kavale, P. Wagh, S. Gupta, and J. Gurav, “Superhydrophobic silica coating by dip coating method,” Applied Surface Science, 277, 67-72, April 2013. https://doi.org/10.1016/j.apsusc.2013.04.001.

[8] A. Goli, B. Rout, T. Cyril, and V. Govindaraj, “Evaluation of Mechanical Characteristics and Plastic Coating Efficiency in Plastic-Modified Asphalt Mixes,” International Journal Pavement Research and Technology, 16(3), 1-12, March 2022. https://doi.org/10.1007/s42947-022-00157-y.

[9] X. Wu, I. Wyman, G. Zhang, J. Lin, Z. Liu, Y. Wang, and H. Hu, “Preparation of superamphiphobic polymer-based coatings via spray- and dip-coating strategies,” Progress in Organic Coatings, 90, 463-471, August 2015. https://doi.org/10.1016/j.porgcoat.2015.08.008.

[10] F. Jia, J. Mao, X. Yang, Y. Ma, and C. Yao, “Thermal,physical and mechanical properties of hydrogenated dimer acid-based Nylon 636/Nylon 66 copolymers,” Chinese Chemical Letters, 24(7), 654-658, May 2013. https://doi.org/10.1016/j.cclet.2013.04.012.

[11] N. Donati, J. C. Spada, and I. C. Tessaro, “Enhancing properties of biodegradable starch-based foams: Influence of polymer coating dissolution solvents in dip coating process,” Progress in Organic Coatings, 194, 108558, September 2024. https://doi.org/10.1016/j.porgcoat.2024.108558.

[12] F. Li, X. Zhang, K. Zhang, F. Li, L. Wang, and J. Cao, “Exploring the effect of different waste polypropylene matrix composites on service performance of modified asphalt using analytic hierarchy process,” Construction and Building Materials, 405, 133292, November 2023. https://doi.org/10.1016/j.conbuildmat.2023.133292.